Dependence of the electrical properties of defective single-walled carbon nanotubes on the vacancy density

Luo Yu-Pin(罗煜聘)[a], Tien Li-Gan(田力耕)[b], Tsai Chuen-Horng(蔡春鸿)[b], Lee Ming-Hsien(李明宪)[c], and Li Feng-Yin(李丰颖)[d]†

[a] *Department of Electronic Engineering, National Formosa University, Yunlin County, Taiwan* 632, *China*

[b] *Department of Engineering and System Science, National Tsing Hua University, Hsin Chu, Taiwan* 300, *China*

[c] *Department of Physics, Tamkang University, Tamsui, Taipei County, Taiwan* 251, *China*

[d] *Department of Chemistry, National Chung Hsing University, Taichung, Taiwan* 420, *China*

(Received 29 November 2010; revised manuscript received 12 January 2011)

The relationship between the electric properties and the vacancy density in single-walled carbon nanotubes has been investigated from first principles as well as the dependence of the influencing range of a vacancy in the nanotube on the nanotube chirality. Compared with the long-range interaction of the vacancies in a single-walled carbon nanotube with non-zero chiral angle, a much shorter interaction was found between vacancies in a zigzag single-walled carbon nanotube. In this study, we investigated the bandstructure fluctuations caused by the nanotube strain, which depends on both the vacancy density and the tube chirality. These theoretical results provide new insight to understand the relationship between the local deformation of a defective single-walled carbon nanotube and its measurable electronic properties.

Keywords: chiral carbon nanotube, mono-vacancy defect, energy gap

PACS: 73.22.–f, 73.63.Fg, 71.15.Mb **DOI:** 10.1088/1674-1056/20/8/087303

1. Introduction

Ever since the demonstration of a carbon nanotube (CNT) as a working transistor,[1] the design and reliability of the circuits made by CNTs have become important issues. In contrast to the prevailing conception of single-walled nanotubes (SWCNTs) as perfectly crystalline wires, even high-quality SWCNTs on average contain one structural defect per 4 μm.[2] However, defective SWCNTs possess interesting electric properties[3] that open up new potential applications in nanodevices. Among the structural defects in SWCNTs, vacancy defects are particularly important in future application since they can be introduced into nanotubes by either ionic or electronic irradiation and their density can be controlled through irradiation doses.[4] In addition, a mono-vacancy defect (MVD) can reduce the drive current by about 28%, regardless of the location of the vacancies in the SWCNTs.[5] Gomez-Navarro *et al.* employed consecutive Ar^+ irradiation doses to generate a uniform density of defects, and thus examined the dependence of the conductance on the vacancy defect density in SWCNTs.[6] Biel *et al.* examined the characteristics of the localization regime in terms of the length, temperature, and density of defects of SWCNTs by averaging over various random configurations of defects for a metallic (10, 10) SWCNT.[7] Furthermore, the results of selected electrochemical deposition reveal that most of the electronic behaviours of a particular CNT transistor are caused by vacancy defects, and are not a characteristic of the CNT itself.[2] Therefore it is essential to understand the electronic structural changes caused by vacancy defects in the future application of SWCNTs. Kim *et al.*[8] considered bandstructure to explain why the electrical characteristics of SWCNTs are modified chiefly by the localized gap states, found far from the band gap edge, produced by vacancy-related defects. These localized gap states, also called 'deep levels', can be spatially resolved by scanning tunneling spectroscopy.[9] The energy gap between the deep levels and the conduction or valence bands can be measured by scanning photoluminescence microscopy.[10] A model to explain the dependence of the electrical conductivity on the vacancy density has been proposed by Baskin *et al.*[11] Both experimental and theoretical findings are beginning to yield a general picture of the vacancy effect on the electrical characteristics

†Corresponding author. E-mail: feng64@nchu.edu.tw

© 2011 Chinese Physical Society and IOP Publishing Ltd

of SWCNTs, but numerous critical issues remain unresolved. For instance, how the structural changes, associated with vacancy defects, affect the electronic structures of SWCNTs, which in turn determine their applications. Furthermore, it is crucial in the design of the circuits made by SWCNTs to distinguish the intrinsic properties due to a vacancy from those caused by the interaction between defects. Hence, a deep understanding of the effects of vacancy defects is urgently needed.

In this study, the variation in the bandstructure of SWCNTs due to the MVD density is investigated by employing the first-principles density functional theory (DFT) calculations. The results characterize the interaction range of a single MVD through SWCNTs of various lengths. The variation in the bandstructure has been investigated via the local energy gap between the deep levels and the valence band maximum (VBM) state at Γ point, which is the minimum in energy along the tube axis. Structural and electronic structure analyses have been undertaken as their results can be directly studied in the experiments. For example, the structural changes can be measured with an atomic force microscope or a scanning tunneling microscope, while the variance of the local energy gap can be examined by scanning photoluminescence microscopy. The effect of defect density on the local energy gap, as defined above, reveals itself through the changes in the hybridization between bands around the Fermi level triggered by structural deformation due to the vacancy defects. These results were adopted to characterize the intrinsic properties of an isolated MVD without the influence of the neighbouring vacancies.

2. Method and model

Three different SWCNTs, (5, 5), (10, 0), and (10, 5), were used to represent armchair, zigzag, and chiral nanotubes, respectively. To elucidate the effect of MVD density on the electrical characteristics of SWCNTs, first, six zigzag SWCNTs were simulated with defect densities of one MVD per 2, 3, 4, 5, 6, and 7 unit cells (40 atoms per unit cell), corresponding to 79, 119, 159, 199, 239, and 279 carbon atoms, respectively. A similar study of five armchair SWCNTs was performed with defect densities of one MVD per 4, 6, 8, 10, and 12 unit cells (20 atoms per unit cell), corresponding to 79, 119, 159, 199, and 239 carbon atoms, respectively. As for the chiral SWCNTs, only one model was generated due to the large unit cell (140 atoms per unit cell), corresponding to 139 carbon atoms. We employed the CASTEP code[12] to compute the electronic properties of these defective SWCNTs.

Each simulated nanotube was placed in a tetragonal supercell with lattice constants a, b, and c. The lattice constants a and b were 20 Å (1 Å = 0.1 nm), preventing interaction between adjacent nanotubes. The lattice constant c along the tube axis was taken to be equal to the one-dimensional lattice parameter of nanotubes. Except where explicitly stated, the typical calculation was as follows. The calculations were done using geometric optimization with the generalized gradient approximation (GGA).[13,14] The structure of the defective nanotube was fully optimized when the force on each atom during relaxation was under $0.005\,\mathrm{eV}\cdot\mathrm{Å}^{-1}$. The nuclei and core electrons were represented by ultrasoft pseudopotentials.[15] The summation was performed over the one-dimensional (1D) Brillouin zone with wavevectors varying only along the tube axis, using k-point sampling and a Monkhorst–Pack grid.[16] A kinetic energy cut-off of 240 eV and 12 k points was used along the z axis to ensure convergence in the calculations. The fast-Fourier-transform (FFT) grid was chosen according to the number of carbon atoms in the particular SWCNT. For example, the FFT grid for the zigzag 79-carbon-atom nanotube was set to be $90 \times 90 \times 40$, and for the armchair 79-carbon-atom SWCNT was set to be $90 \times 90 \times 45$, and for the chiral 139-carbon-atom SWCNT was set to be $90 \times 90 \times 50$.

3. Results and discussion

After structural optimization, each MVD in all models becomes a so-called 5-1DB defect with two of its three adjacent dangling bonds (DB) in an ideal MVD, recombining with each other to yield a pentagon ring with the remaining DB unchanged. The newly formed carbon–carbon bond tilts about the tube axis for armchair tubes. However, it is perpendicular to the tube axis for zigzag tubes. These results are the same as those found in Ref. [17]. Interestingly, for chiral tubes, this carbon–carbon bond always tilts about the tube axis.

The structural deformation associated with variation in MVD densities is analysed by calculating the oblateness, which is measured by dividing the largest diameter of the ring containing the twofold coordinated carbon atoms by the shortest diameter of the same ring of the defective SWCNTs, as shown in Fig. 1 by using the (10, 0) and (5, 5) SWCNTs as examples.

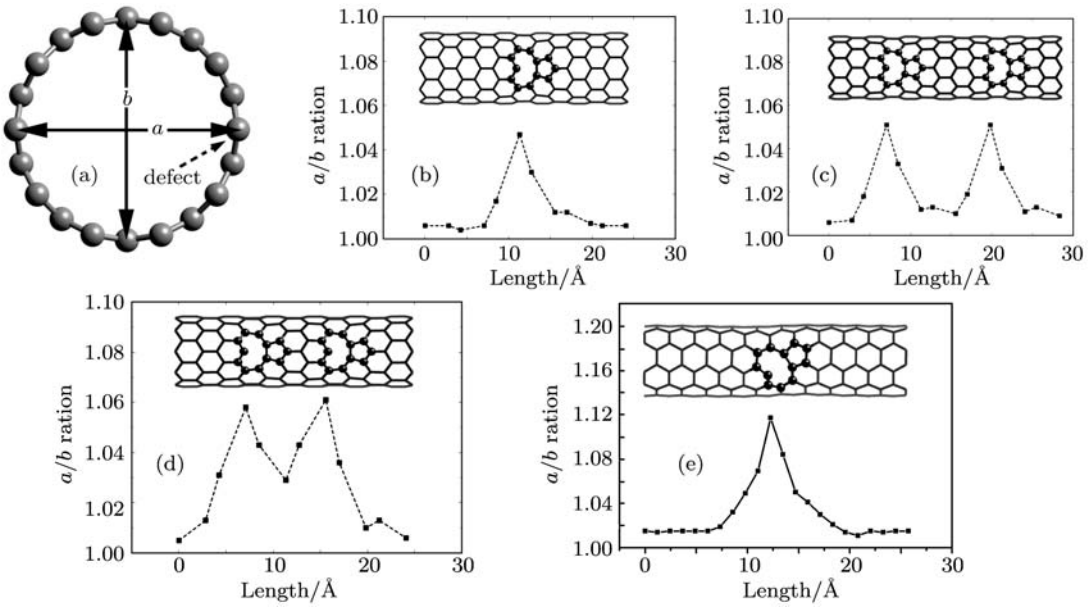


Fig. 1. The oblateness variation of defective (10, 0) and (5, 5) SWCNTs along the tube axis. Panel (a) is a schematic plot to indicate the axes for the oblateness calculation. Panel (b) is the oblateness variation in the model of 239 carbon atoms with one MVD in a defective (10, 0) SWCNT, a fully relaxed example. Panel (c) is that in the model of 278 atoms with two MVDs in a defective (10, 0) SWCNT, an example almost relaxed. Panel (d) is that in the model of 238 atoms with two MVDs in a defective (10, 0) SWCNT, a non-relaxed example. And panel (e) is the oblateness variation in the model of 239 carbon atoms with one MVD in a defective (5, 5) SWCNT.

The results presented in Table 1 reveal that the zigzag SWCNT bulges to form an elliptical shape around the MVD, and slowly relaxes to more rounded shapes away from the MVD. With increasing defect density, the distortion of zigzag SWCNTs increases but the local energy gap declines. Coincidently, both the local energy gap and the oblateness converge when the model includes more than 159 carbon atoms, corresponding to the distance between any two nearby vacancy defects over 16.98 Å. Puzzling as these results appear, they can actually be integrated to resolve several important issues in future applications of vacancy-defective zigzag SWCNTs, such as the influencing range of an MVD and variation in electrical properties due to vacancy defects. The oblateness along the tube axis with various models is plotted in Fig. 1 to characterize the influencing range of an MVD. Clearly, the oblateness decreases from its highest value in the twofold coordinated carbon to approximately unity if the neighbouring defects are far away. The influencing range is about 17 Å on the five-member ring sides of 5-1DB, and 12 Å on the other side. Therefore, the vacancy interaction in zigzag SWCNTs is rather short-ranged.

As to armchair nanotubes with different lengths, our calculations also confirm these findings as shown in Table 2: when the vacancy density increases, the distortion of the defected armchair SWCNTs increases also. Similar to those found in the zigzag SWCNTs, the armchair SWCNT bulges

Table 1. Oblateness and bandgap of zigzag (10, 0) SWCNT with a single mono-vacancy defect. Parameter a is the diameter of the ring that contains the twofold coordinated carbon, as shown in Fig. 1, and b is the diameter in the same ring as diameter a but perpendicular to it.

Model size	a/Å	b/Å	Oblateness	Protruding angle	Local energy gap [a]/eV
80 [b]	7.943	7.926	1.002	16.0 [c]	0.67
79	8.416	7.511	1.120	35.1	0.19
119	8.194	7.749	1.057	33.2	0.29
159	8.115	7.747	1.048	29.8	0.39
199	8.154	7.745	1.052	31.5	0.39
239	8.114	7.751	1.047	30.3	0.41
279	8.116	7.748	1.047	29.5	0.40

[a] The energy gap between the deep level state and valence band maximum state.
[b] Perfect (10, 0) SWCNT for comparison.
[c] The diameter is averaged over the rings in a perfect (10, 0) SWCNT, since no DBs are present.

Table 2. Oblateness and bandgap of armchair (5, 5) SWCNT with single mono-vacancy defect.

Number [a]	Oblateness [b]	Length variation [c]	Protruding angle	Local energy gap/eV
79	1.150	0.023	28.5	0.098 (D [d])
119	1.122	–0.001	38.5	0.145 (I [e])
159	1.115	–0.006	38.5	0.000
199	1.112	0.008	37.5	0.065 (I [e])
239	1.117	–0.011	37.6	0.073 (D [d])

[a] Number of carbon atoms per one mono-vacancy defect; [b] oblateness measured around the vacancy site; [c] the difference in the lattice constant c of the defected SWCNTs before and after structural optimization; [d] direct bandgap; and [e] indirect bandgap.

around the MVD to form an elliptical shape, and slowly relaxes to more rounded shapes away from the MVD, as shown in Fig. 1(e). The relaxation of the structural deformation due to 5-1DB can be treated as an index to measure the influencing range of a vacancy in SWCNT. Within 15 Å from the 5-1DB site, the oblateness relaxes close to one rather fast, but with rather long tail even beyond the length of our largest model. Compared with the short-range interaction between vacancy defects in zigzag SWCNTs, the vacancy interaction in armchair SWCNTs is long-range interaction, consistent with those found in Ref. [17].

The strain induced by the vacancy defect can be estimated by two factors, i.e., the length variation and the protruding angle. The length variation of the defective SWCNTs can be defined as the difference between the lattice constant along the tube axis before and after the structural optimization. The positive length variation indicates that the tube length expands after structural optimization. Closely examining the length variation of the defective armchair SWCNTs with various MVD densities, as presented in Table 2, reveals that formation of 5-1DB from an ideal vacancy can either shrink or expand the length of a defective armchair SWCNT as the defect density increases. However, the tube length of the defective zigzag SWCNT decreases slightly as the MVD density increases, quite different from that found in the defective armchair SWCNT. The length variation measures the overall strain, while the protruding angle measures the local strain with the twofold coordinated carbon protruding out of the tube, as defined in Fig. 2. Closely examining the local structure of the 5-1DB defects with various MVD densities in a zigzag SWCNT, as presented in Fig. 3(b), reveals that 5-1DBs shrink as the defect density increases. This shrinkage in turn causes the twofold coordinated carbon to protrude away from the tube, as characterized by the protruding angle. However, in the defective armchair SWCNTs, the protruding angle does not vary a lot except in the high defect density. These results explain why the tube length shrinks for zigzag SWCNTs but the tube length of the armchair SWCNTs fluctuates just a little bit. Furthermore, there is no obvious correlation between the vacancy density and the local energy gap. Interestingly, the bandstructures of the defective armchair SWCNTs, as shown in Fig. 4, indicate that the valence band maximum (VBM) state and the conduction band maximum (CBM) state fluctuate among different mono-vacancy defect densities. Therefore this local energy gap is not sufficient to describe the change in the bandstructure in armchair SWCNTs due to mono-vacancy defect densities.

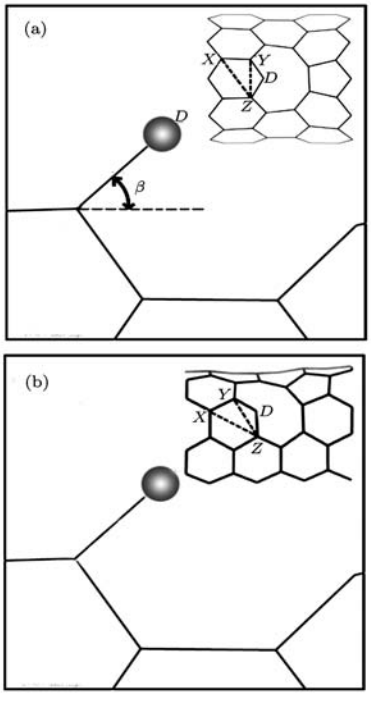


Fig. 2. A schematic plot for the protruding angle for SWCNTS. Panel (a) is for a zigzag SWCNT and (b) is for an armchair SWCNT. As viewed from the ZY direction, the protruding angle is defined as the twist angle between the two planes constructed by YDZ and XYZ, respectively, where D is the twofold coordinated carbon.

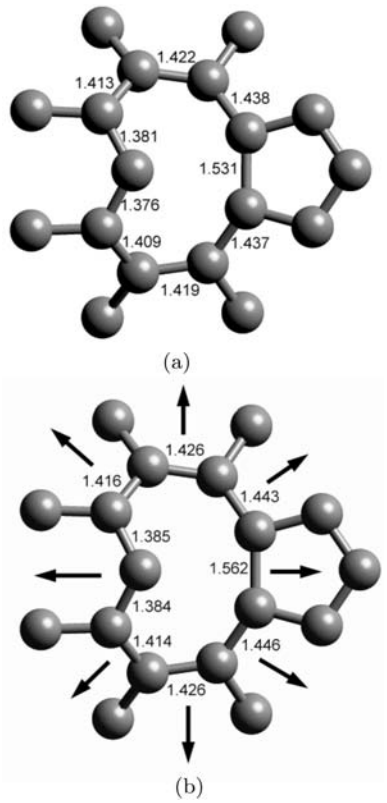


Fig. 3. Local structure of the 5-1DB defect in a (10, 0) SWCNT, where panel (a) is the structure of the model with 79 carbon atoms and (b) is that with 119 atoms.

Compared with the complicated behaviours of the defective armchair SWCNTs, the defective zigzag SWCNTs do show certain trends as the defect density increases, such as the density of state (DOS) for three different MVD densities in (10, 0) SWCNT, as shown in Fig. 5. Clearly the Fermi level lies between the deep levels and the VBM state, and not only does the local energy gap shrink but also the deep level becomes broader as the MVD density increases. Obviously the properties of the defective SWCNTs strongly depend on the tube's chirality. In order to verify this chirality dependence, we also performed a similar calculation using a single-walled (10, 5) nanotube modeled by 140 carbon atoms with one carbon atom missing. It can be expected that the structural properties of defective chiral SWCNTS should be more like those of defective armchair SWCNTs, rather than the defective zigzag SWCNTs, since the zigzag ones have zero chiral angle. For example, the MVD also forms 5-1DB with the newly formed C–C bond tilt about the tube axis, similar to that found in the armchair SWCNTs. The influence range of the 5-1DB in this chiral SWCNT is also a long-range one, just like the armchair SWCNTs, covering the entire tube length. The tube length does not change a lot, just like the defective armchair SWCNTs. However, the bandstructure of the defective chiral (10, 5) SWCNTs is more like that of the defective zigzag (10, 0) SWCNTs due to their semiconducting characterisitics, as shown in Fig. 6. The local energy gap of the defective chiral (10, 5) nanotube between the VBM state and the local gap state is 0.3 eV at the point of the Brillouin zone, smaller than the bandgap of the corresponding perfect (10, 5) nanotube, 0.722 eV, due to a defective band just above the Fermi level, similar to those found in zigzag defective SWCNTs.

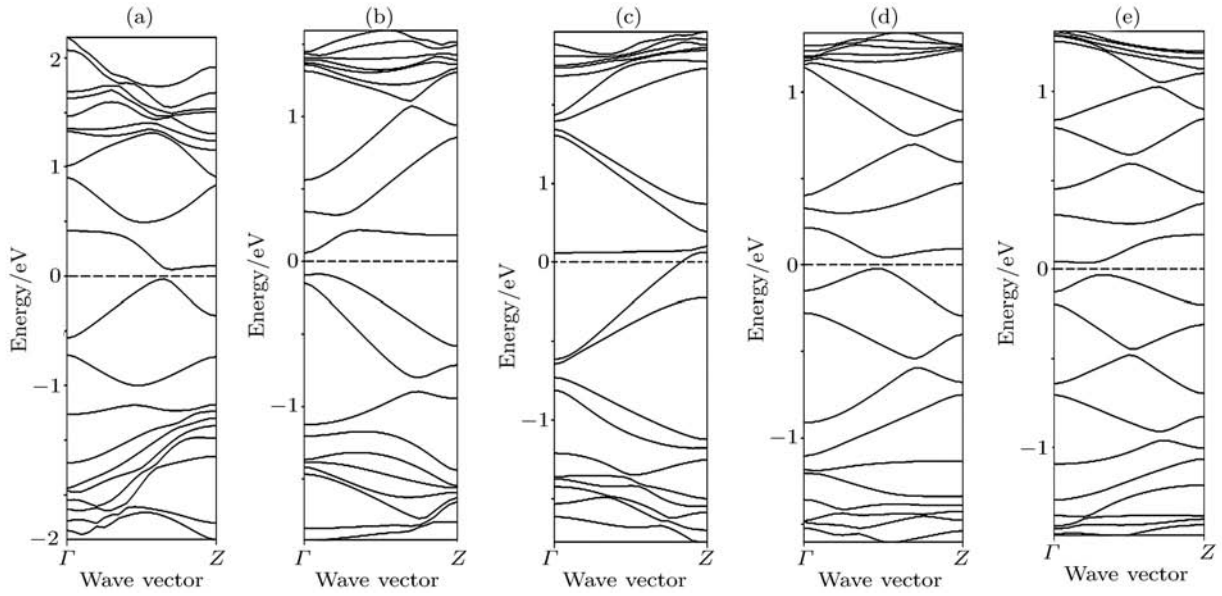


Fig. 4. The bandstructures of the single mono-vacancy defective (5, 5) armchair carbon nanotube with various numbers of carbon atoms: (a) 79, (b) 119, (c) 159, (d) 199, and (e) 239 carbon atoms.

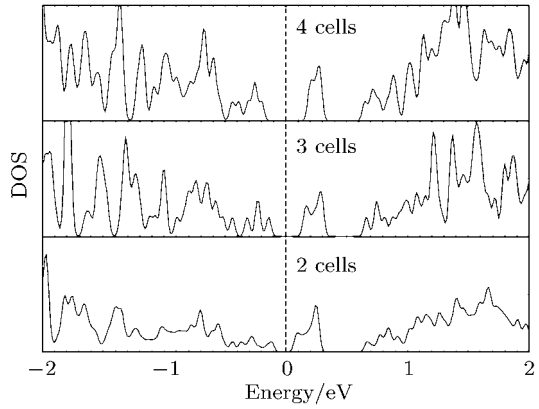


Fig. 5. The DOS for three different MVD densities in a (10, 0) zigzag SWCNT. The band gaps between VBM and CBM states for 2, 3, and 4 unit cells are 0.792, 0.809, and 0.849 eV, respectively.

In order to explain the variance of the electronic structure for these defective SWCNTs, the local partial density of state (LPDOS) calculation of a defective zigzag (10, 0) SWCNT was performed as an example. We analysed those rings around the 5-1DB, as presented in Fig. 7, to understand the effects of structural deformation on the electronic structure of SWCNTs, where the 2P orbitals of carbon atoms are dissected into two categories: along the tube axis (P_z) and radial components (P_x and P_y). Our results indicate that the VBM state is composed mostly of the P_x and P_y orbitals of all the carbon atoms. However, in MVD density, the deep levels are composed of the P_z orbital of the twofold coordinated carbon and the P_x and P_y orbitals of the alternative rings, including the ring with the newly formed C–C bond. Therefore, at least in high MVD density, the charge density of the deep levels is not only localized in the three carbon atoms surrounding the MVD but also includes the P_x and P_y orbitals of the alternative rings around the vacancy site. Given the orbital distributions, the interaction between the twofold coordinated carbon and the rest of the carbon atoms substantially influence the bandstructure of the nanotube, and especially the deep levels.

By putting all these results together, the overall picture emerges. At high defect density, in order to release the strain caused by the surrounding defects, the 5-1DB shrinks and then causes the twofold coordinated carbon to protrude out of the SWNCT to have a high protruding angle. Therefore, the oblateness along the tube axis also increases. These structural changes increase the interaction between the twofold coordinated carbon and its surrounding atoms, and, in turn, cause the deep levels to broaden and the local energy gap to shrink. Therefore the local energy gap can be characterized by the protruding angle of the twofold coordinated carbon, such that a large protruding angle is associated with a small energy gap and large oblateness. This finding reveals that as the protruding angle increases, the energy of the deep levels falls, shrinking the local energy gap. Therefore, it clarifies the relationship between the variation of the local energy gap and the MVD density. As to the defective armchair SMCNTs, the variation in the local energy gap due to the MVD density is similar to that found in defective zigzag SWCNTs but more sensitive due to the long-range interaction between MVDs.

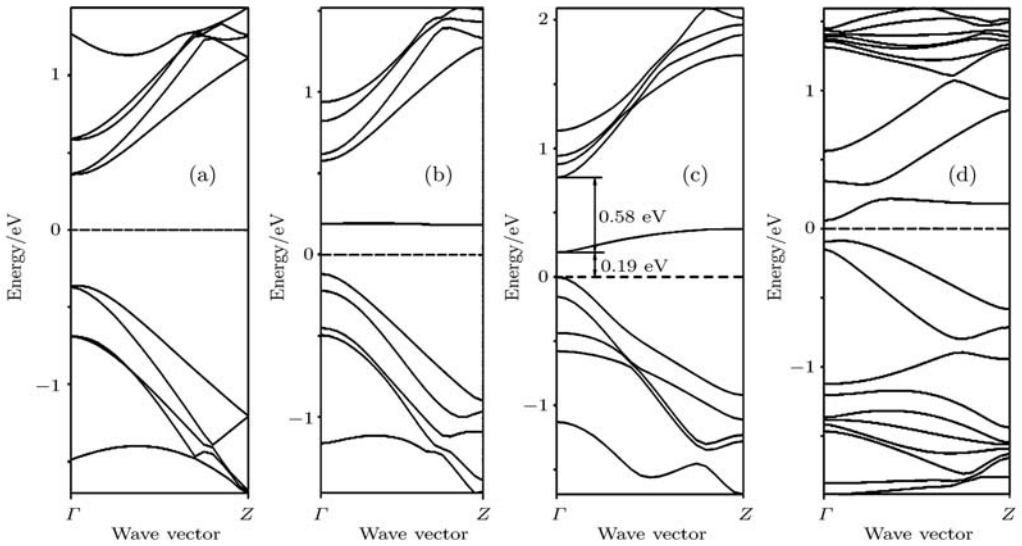


Fig. 6. The bandstructures of a defective chiral SWCNT compared with defective zigzag and armchair SWCNTs: (a) the band structure of a perfect chiral (10, 5) SWCNT, (b) the band structure of a defective chiral (10, 5) SWCNT with a mono-vacancy defect, (c) the band structure of a defective zigzag (10, 0) SWCNT with a mono-vacancy defect and (d) the band structure of a defective armchair (5, 5) SWCNT with a mono-vacancy defect. The dashed line indicates the Fermi level.

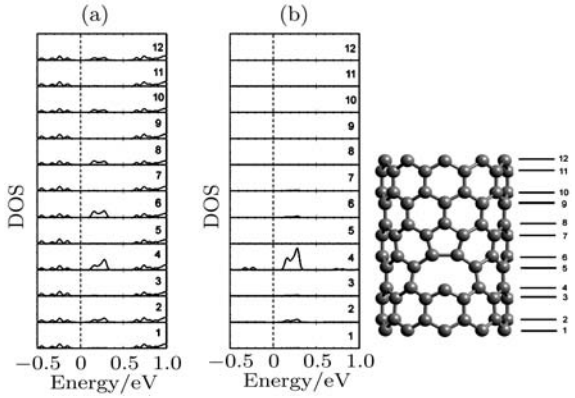


Fig. 7. LPDOS of a (10, 0) SWCNT with one MVD for a three-unit system (119 carbon atoms). Those carbon atoms forming a circle perpendicular to the tube axis are grouped together as one analysis set for the LPDOS analysis and are defined as one layer. There are twelve layers, as defined in the plot on the right. Panel (a) is the LPDOS for the P_x and P_y orbitals of the carbon atoms in the particular layer, where the dashed line is the Fermi level. Panel (b) is the LPDOS for the P_z orbitals of the carbon atoms in the layer. The twofold coordinated carbon is in the fourth layer and the newly formed C–C bond is in the sixth layer.

4. Conclusion

This study provides theoretical support for analysing the influence of an isolated single vacancy defect in SWCNTs with regard to their structural and electrical properties, including zigzag, armchair, and chiral types. The relationship between the local energy gap and the MVD density was elucidated by our calculations from first principles. The bandstructure of an SWCNT is sensitive to MVD density and the influence of the MVDs strongly depends on its chirality. However, no simple correlations between the MVD density and the local energy gap are found.

The influencing range of an MVD is characterized by structural deformation analysis, and then a microscopic explanation is offered to relate the structural deformation to the local energy gap variation. The strain increases with the defect density, subsequently increasing the oblateness, causing the twofold coordinated carbon to protrude outward and, ultimately, reducing the local energy gap. This explanation interprets all data in Table 1 coherently, and rationalizes the variation in local energy gap with MVD density.

Our results suggest that the SWCNT's intricate properties can be tuned by controlling the MVD density. This study can shed some light on modulating the local energy gap via ion irradiation for future potential applications.

Acknowledgements

The authors would like to acknowledge the National Centre for High-Performance Computing, Taiwan in providing computational resources. Financial support from National Science Council (NSC) of Taiwan is gratefully acknowledged. Li F Y is grateful for the support of NSC 96-2113-M-005-008-MY3, Lee M H acknowledges the support of NSC 95-2112-M-032-015, and Tsai C H is grateful for the support of NSC 95-2120-M-007-007. Discussions with professor A. Proykova are acknowledged.

References

[1] Tans S J, Verschueren A R M and Dekker C 1998 *Nature* (London) **393** 49
[2] Fan Y, Goldsmith B R and Collins P G 2005 *Nature Mater.* **4** 906
[3] Tien L G, Tsai C H, Li F Y and Lee M H 2005 *Phys. Rev.* B **72** 245417
[4] Gomez-Navarro C, De Pablo P J, Gomez-Herrero J, Biel B, Garcia-Vidal F J, Rubio A and Flores F 2005 *Nature Mater.* **4** 534
[5] Neophytou N, Kienle D, Polizzi E and Anantram M P 2006 *Appl. Phys. Lett.* **88** 242106
[6] Biel B, Garcia-Vidal F J, Rubio A and Flores F 2005 *Phys. Rev. Lett.* **95** 266801
[7] Kim G, Jeong B W and Ihm J 2006 *Appl. Phys. Lett.* **88** 193107
[8] Lee S, Kim G, Kim H, Choi B Y, Lee J, Jeong B W, Ihm J, Kuk Y and Kahng S J 2005 *Phys. Rev. Lett.* **95** 166402
[9] Milkie D E, Staii C, Paulson S, Hindman E, Johnson A and Kikkawa J M 2005 *Nano Lett.* **5** 1135
[10] Baskin E, Reznik A, Saada D, Adler J and Kalish R 2001 *Phys. Rev.* B **64** 224110
[11] Payne M C, Teter M P, Allan D C, Arias D C and Johannopoulos J D 1992 *Rev. Mod. Phys.* **64** 1045
[12] Perdew J P, Chevary J A, Vosko S H, Jackson K A, Pederson M R, Singh D J and Fiolhais C 1992 *Phys. Rev.* B **46** 6671
[13] White J A and Bird D M 1994 *Phys. Rev.* B **50** 4954
[14] Vanderbilt D 1990 *Phys. Rev.* B **41** 7892
[15] Monkhorst H J and Pack J D 1976 *Phys. Rev.* B **13** 5188
[16] Lu A J and Pan B C 2004 *Phys. Rev. Lett.* **92** 105504
[17] Kotakoski J, Krasheninnikov A V and Nordlund K 2006 *Phys. Rev.* B **74** 245420